Theor Chem Acc (2012) 131:1188
DOI 10.1007/s00214-012-1188-9

REGULAR ARTICLE

Impact of DFT functionals on the predicted magnesium–DNA interaction: an ONIOM study

José P. Cerón-Carrasco · Alberto Requena · Denis Jacquemin

Received: 29 June 2011 / Accepted: 9 September 2011 / Published online: 10 March 2012

Abstract We investigate the descriptions of several density functional theory functionals in modeling the interactions between DNA and magnesium, the divalent cation with the largest intracellular concentration. Precisely, the metal-induced proton transfer (PT) in the guanine-cytosine base pairs is analyzed within an hybrid two-layers QM/QM approach (ONIOM) by combining several functionals: BP86, B3LYP, B97-D, ωB97x-D and M06-2X, as well as the MP2 approach. The aqueous environment is simulated through, on the one hand, explicit solvent molecules present in the first hydration shell and, on the other hand, the well-known polarizable continuum model for the effects of solvation beyond this first shell. Calculations with all methods indicate that the Mg^{2+} cation coordination to DNA promotes a single PT reaction from the guanine to the cytosine base, characterized by a low back-reaction barrier. M06-2X and ωB97x-D functionals provide consistent results for the simulation of PT reactions. These methods can be combined with B97-D functional in ONIOM partition for the description of the stacking effects.

Dedicated to Professor Vincenzo Barone and published as part of the special collection of articles celebrating his 60th birthday.

J. P. Cerón-Carrasco · D. Jacquemin (✉)
CEISAM UMR CNRS 6230, Université de Nantes,
2, rue de la Houssinière, BP 92208,
44322 Nantes Cedex 3, France
e-mail: denis.jacquemin@univ-nantes.fr

J. P. Cerón-Carrasco
e-mail: jose.ceron@univ-nantes.fr

A. Requena
Departamento de Química Física,
Facultad de Química, Universidad de Murcia,
30100 Campus de Espinardo, Murcia, Spain

Keywords DNA · Magnesium · Tautomerism · Density functional calculations · ONIOM

1 Introduction

Although DNA is protected by the surrounding cellular environment, it is constantly exposed to external agents that may induce variations of its nature and hence alter its biological functions. In that framework, Prof. Barone and collaborators have demonstrated that theoretical chemistry provides a useful and deep understanding of the interactions between UV–visible radiation and DNA. Their studies unravel the nature of the excited state of nucleic acids [1–5] and the subsequent implications for life that they rationalize as radiation-induced changes in DNA canonical structure [6–8]. Interestingly, not only external factors might tune the biological functions of DNA but natural components such as metallic cations (mainly Na^+, K^+, Ca^{2+}, and Mg^{2+}) also play a major role in the stabilization (or unstabilization) of the double-helix structure [9]. Among these compounds, magnesium can be considered as one of the most important because it is present in most of nucleic acids activation processes [10–12]. Furthermore, recent studies suggested that the Mg^{2+}–DNA interaction is a prerequisite for the activity and therapeutic efficiency of some antitumorals drugs, such as mithramycin [13–19]. However, at high concentrations, metals, including Mg^{2+}, may play an opposite role by distorting the DNA structure or by inducing tautomeric changes in the base pairs, which might eventually yield an error in the genetic information [20–23]. It is therefore unsurprising that the influence of cations in life tissues has attracted a considerable attention and has initiated numerous experimental [24–28] and theoretical studies [29–37] aiming to unravel the biological consequences of such metal–nucleic acids interactions.

For DNA, it is well-recognized that metal cations are predominantly coordinated to the guanine–cytosine (GC) base pairs and more precisely on the N7(G) site [38, 39] (see Fig. 1). As a possible consequence of this binding, the amount of so-called rare tautomers, that is, structures arising from exchanging protons with respect to the original canonical form, might be increased [23]. Indeed, though proton transfer (PT) reactions in DNA are energetically unfavorable in the absence of external perturbations [40–50], metalation at N7(G) can possibly activate the transfer of the H1 proton from the N1(G) position to N3(C) leading to a rare tautomer form [51–57]. For the Mg^{2+} cation, Šponer and co-workers have evaluated the importance of PT mechanism on the global mutagenicity of DNA [58]. In agreement with experiments [52, 53], their calculations on deoxyribonucleotide monophosphate–GC model indicate that Mg^{2+} cation promotes the transfer of H1 proton between GC base pair. However, as these authors pointed out, a more refined DNA model is necessary to quantify the Mg^{2+}-induced PT energetic profile [58]. Indeed, for free DNA, we have recently demonstrated that this mechanism is qualitatively changed when the base stacking and confinement effects are considered [59].

In this work, we assess density functional theory (DFT) approaches in the framework of simulations of the interactions between the DNA molecule and the Mg^{2+} cation. Specifically, we test the impact of the functional in the predicted metal-induced H1 PT in the tautomeric equilibrium connecting the canonical system to the rare tautomer, hereafter denoted simply as Mg–GC and Mg–GC1, respectively. This paper is divided as follows: in Sect. 2, we describe the theoretical methods employed for the treatment of metal–DNA interactions; in Sect. 3, we explore the results of different functionals for describing the induced PT reaction and the biological implications of the metal–DNA interaction.

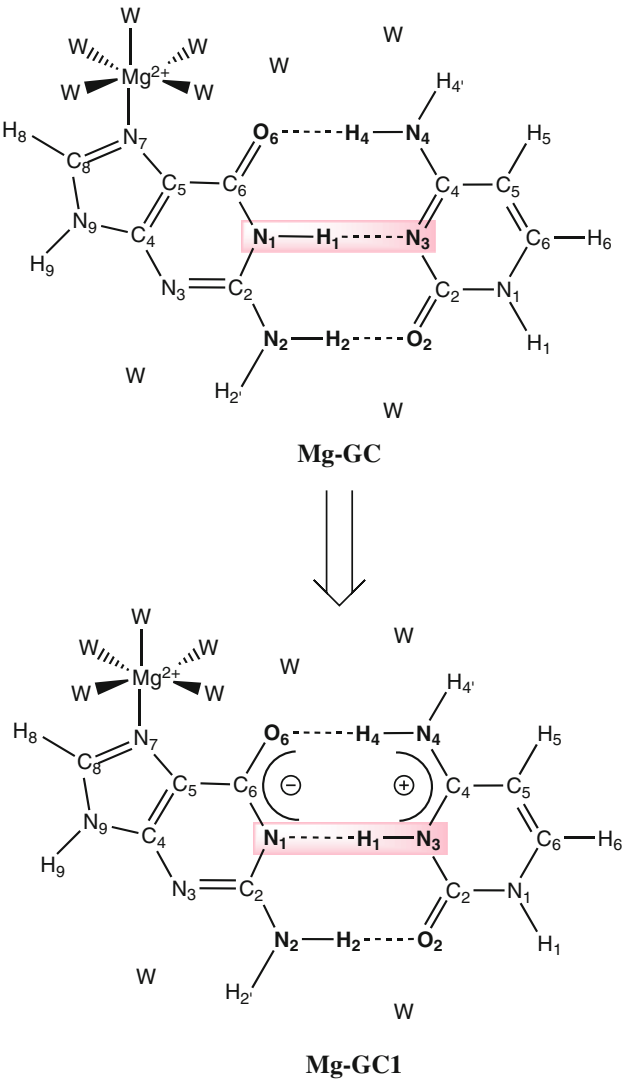

Fig. 1 Structure of the hydrated Mg^{2+}–GC complex and atomic numbering. Mg–GC and Mg–GC1 refers to the canonical and rare tautomer forms, respectively. The transferred proton in the central hydrogen bond is highlighted in *pink*. The explicit water molecules of the first hydration shell around the magnesium cation and the GC pair are shown as W

2 Computational methods

The DNA structure and properties are mainly governed by two non-covalent interactions: interbase bonds and base stacking [60–62]. As recently demonstrated by Acosta-Silva et al. [63], these two interactions are not independent. Consequently, to obtain reliable predictions of the DNA changes induced by the Mg^{2+}, an adequate treatment of both interactions is needed. The minimum DNA fragment able to cover the stacking influence on interbase bonds is a three base pair sequence, where a central base pair is under the influence of two neighboring bases pairs, located below and above the investigated moiety [64]. Here, a DNA trimer model is built up by inserting the Mg^{2+}–GC system into a double-stranded B-form trimer d(5′-GGG-3′)d(3′-CCC-5′) inspired by the study of DNA's radical anion of Chen et al. [65]. As solvent affects both the metal bonding and the GC tautomeric equilibrium [66, 67], we have combined the first hydration shell of Mg^{2+} cation with the first hydration shell for the GC base pair. For the former, the Mg^{2+} cation exists in its hexahydrated form in bulk water, but it looses one water molecule when bonded to N7(G) of the nucleotide, and therefore five explicit water molecules are included to saturate the first hydration shell of the cation [68]. For the latter, four water molecules have been placed in the vicinity of the N3(G), O6(G), O2(C), and N4(C), which is a suitable representation of the experimentally observed hydration shell of the GC base

pair embedded in DNA [69] and is also consistent with previous molecular dynamics simulations [70, 71]. Accordingly, nine explicit water molecules are included in our model as shown in Fig. 1. Since lateral sugar-phosphate backbones are known to have a trifling influence on the PT reactions [59, 64], only the base pairs are included in the model, subsequently allowing to test several theoretical schemes. The resulting model is shown in Fig. 2 and allows a straightforward partition of the molecular system in two well-defined regions: (1) the central GC base pair, the Mg^{2+} cation and all explicit water molecules (in ball-and-sticks), and (2) the two GC neighboring bases (in tube). These two regions have been described within the partitioning approach developed by Morokuma and co-workers (ONIOM) [72] as implemented in Gaussian09 [73]. When the ONIOM scheme is adopted the choice of the combined methods become a crucial factor. From a theoretical point of view, CCSD(T) is the reference method [74]. Based on the rather similar dependences with respect to the basis set of CCSD(T) and MP2 energies, Hobza and Šponer proposed to use the difference between CCSD(T) and MP2 energies computed with medium basis to extrapolate the CCSD(T)/CBS, where CBS refers to the complete basis set limit [75]. Unfortunately, even within this approach, the CCSD(T) calculations are beyond reach for large systems as the one required in our investigation (115 atoms). As alternative, the DFT methods provide a computational tractable approach to biological systems. However, though early functionals provide a quite acceptable description for the covalent bonds, they fail to model correctly dispersion energy that is essential to describe the stacking effect and are not always very efficient for H-bonds [76, 77]. To partially overtake these limitations, Grimme proposed a dispersion corrected DFT scheme (DFT-D), where an empirical C_6R^{-6} term is added to usual DFT equations [78]. With this correction, DFT methods can be successfully applied to study intermolecular interactions in biological systems [79–82]. Additionally, novel *meta*-hybrid functionals developed by Zhao and Truhlar, and more precisely the M06-2X variation, have also been shown to adequately model non-covalent interactions [83–85].

To evaluate the impact of the selected functional in the study of magnesium–DNA interaction, pure (BP86 [86, 87]), pure dispersion corrected (B97-D [88]), hybrid (B3LYP [89, 90]), *meta*-hybrid (M06-2X [91]), and range-separated dispersion corrected (ωB97X-D [92]) functionals are combined as summarized Table 1. We should note that the inclusion of high percentage of Hartree–Fock exchange in the functional might be problematic in certain cases as transition metals [85]. However, they can be successfully used for the study of light element like Mg. For instance, the good performance of M06-2X functional (54% of exact exchange) has been demonstrated in a study of the absorption of CO on MgO surfaces [93]. The listed functionals are combined with the 6-311++G(d,p) and 6-31+G(d) basis sets for the description of the atoms in the high and low layers, respectively. For each scheme, we follow the H1 proton exchange by scanning the H1–N3(C) bond distance. More specifically, the ONIOM potential energy curves are computed through the partial optimization of the high layer (the H1–N3(C) distance is fixed along the scanning), whereas atoms in the low layer are frozen in space because their relaxation is expected to have a minor effect on the whole energy profile [64, 65]. In a second step, the resulting three critical points in the energy curves, namely the two minima and the maximum, are selected as starting point for a full optimization of the high layer, keeping the restriction in the low layer. Although the

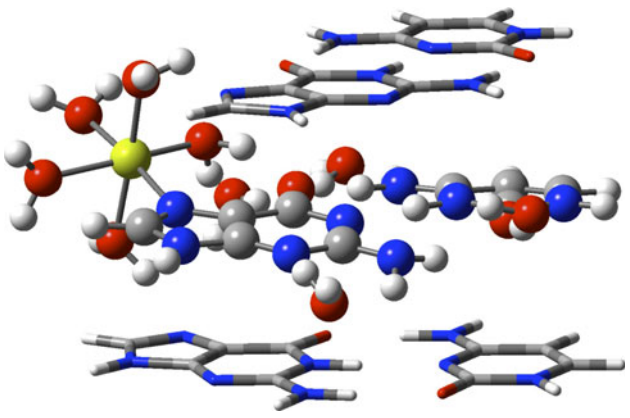

Fig. 2 Designed DNA fragment. The central Mg^{2+}–GC complex corresponding to the high layer level in the ONIOM scheme is represented with balls-and-sticks. The border base pairs confining the central GC included in the low layer, are displayed in tube

Table 1 Theoretical methods for the description of the high and low layer within the two-layers ONIOM approach

Method	High layer[a]	Low layer[b]	PCM
1	M06-2X	B97-D	–
2	ωB97X-D	B97-D	–
3	B97-D	B97-D	–
4	B3LYP	B97-D	–
5	BP86	B97-D	–
6[c]	MP2/6-31G(d)(0.25)		–
7	M06-2X	M06-2X	–
8	M06-2X	PM6	–
9[c]	M06-2X	B97-D	Single-point
10	M06-2X	B97-D	Optimization

[a] Combined with the 6-311++G(d,p) basis set

[b] Combined with the 6-31+G(d) basis set

[c] Single-point calculation using the geometry of method 1

vibrational calculations in non-stationary points (frozen low layer) should be analyzed cautiously, the absence of imaginary frequency for minima (Mg–GC and Mg–GC1) and presence of a single imaginary mode for the transition state (Mg–GC1‡) related to the H1–N3(C) stretching confirm the nature of the structures. The vibrational corrections obtained in the same approximate way have been used to estimate the Gibbs energies. Additional MP2 calculations have been carried out, that is the energy of hydrogen bonding and stacking interactions was calculated through a MP2/6-31G(d)(0.25) single-point calculation on the geometries obtained through method 1. In the 6-31G(d)(0.25) basis set, originally proposed by Hobza and Šponer [94, 95], a more diffuse polarization *d*-functions are used for the element belonging to the first period by replacing the exponent of 0.80 by 0.25 in the standard Pople's basis set to account for dispersion attraction. This choice provides an improved description for base stacking in nucleic acids at a reasonable computational cost [96, 97] but remains less potent than 6-311++G(d,p). Finally, since solvent affects both the metal bonding and the GC tautomeric equilibrium [98–100], the influence of aqueous environment beyond the first hydration shell has been also assessed by including the well-known polarizable continuum model (PCM) [101–103] in our model following two strategies. On the one hand, PCM corrections are included through single-point energy calculations performed on the optimized geometries, and on the other hand, PCM optimizations have been carried out.

3 Results and discussion

3.1 The high-layer method

As shown Table 1, methods 1–5 have been designed to assess the impact of the high-layer method (M06-2X, ωB97X-D, B97-D, B3LYP, and BP86) on the global PT reaction, the low layer being treated through the dispersion corrected B97-D functional. The computed potential energy curves along H1 PT are represented in Fig. 3 whereas the hydrogen bond distances and relatives energies for the optimized high layer are collated in Table 2. All selected theoretical methods predict the canonical Mg–GC structure to be more stable than the rare tautomer form, Mg–GC1, and do provide a similar picture for the changes in the interbase bonds pattern related to the PT. The major effect of the H1 PT is a shortening of the O6(G)–N4(C) and N1(G)–N3(C), whereas the N2(G)–O2(C) bond is slightly elongated. However, the inspection of Fig. 3 reveals significant differences in the energetic profiles showing the impact of the selected DFT functionals on the description of DNA interactions.

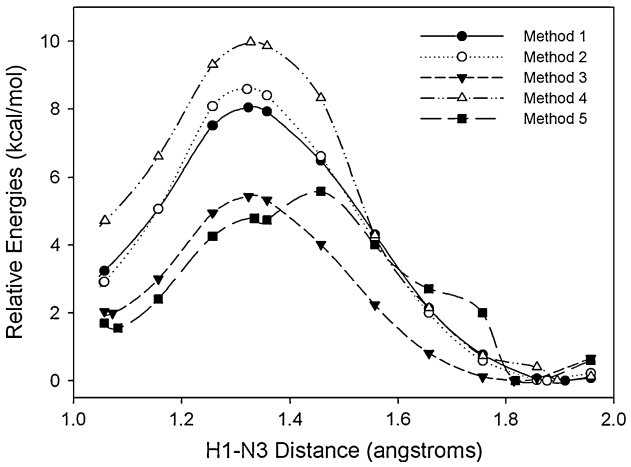

Fig. 3 ONIOM potential energy curves along the H1 proton transference

Table 2 Computed relative energies (ΔE in kcal/mol) along H1 proton transfer with selected high-layer methods. The interbase bonds (in Å) are also listed

	Method				
	1	2	3	4	5
Mg–GC					
ΔE	0.00	0.00	0.00	0.00	0.00
O6(G)–N4(C)	2.84	2.80	2.79	2.83	2.79
N1(G)–N3(C)	2.95	2.92	2.87	2.94	2.88
N2(G)–O2(C)	2.98	2.96	2.91	2.96	2.91
Mg–GC1‡					
ΔE	8.04	8.58	5.44	9.97	5.58
O6(G)–N4(C)	2.65	2.63	2.65	2.65	2.65
N1(G)–N3(C)	2.69	2.68	2.68	2.69	2.68
N2(G)–O2(C)	2.91	2.92	2.90	2.93	2.87
Mg–GC1					
ΔE	3.24	2.91	1.99	4.71	1.55
O6(G)–N4(C)	2.67	2.67	2.67	2.67	2.66
N1(G)–N3(C)	2.87	2.87	2.84	2.88	2.84
N2(G)–O2(C)	3.03	3.03	2.98	3.05	3.00

Let us start by analyzing the results obtained with the more recently designed M06-2X and ωB97X-D functionals, methods 1 and 2, respectively. Since both M06-2X and ωB97X-D have been shown to accurately reproduce non-covalent interactions in biomolecules [104–108] and, specifically, the stacking in DNA [109, 110], it is expected that methods 1 and 2 provide an accurate description of the induced PT reaction. It is therefore satisfying that these two functionals yield extremely similar results, as evidenced by the potential energy curves in Fig. 3 and the relative energies in Table 2. When both layers are described with the B97-D functional (method 3), the generated potential

energy curve significantly differs from the ones produced by the M06-2X and ωB97X-D functionals. Indeed, while M06-2X and ωB97X-D locate the transition state ca. 8 kcal/mol above the canonical structure, the corresponding B97-D value is ca. 5 kcal/mol. A similar trend is found for the relative energy of the rare tautomer, which lies ca. 3 kcal/mol above the canonical structure with M06-2X and ωB97X-D, in contrast with the ca. 2 kcal/mol prediction of B97-D. This dissimilarity can be analyzed in terms of the definition of these three models. B97-D is a local functional, whereas in M06-2X and ωB97X-D, exact exchange is added which generally yields larger (and more realistic) transition energies. Indeed, as Barone et al. demonstrated that the inclusion of exact exchange improves the description of hydrogen bonds and provides more accurate PT energies [111, 112].

Turning to the most widely used functional, namely B3LYP (method 4), sizable energetic barrier (9.97 kcal/mol) and rare tautomer energies (4.72 kcal/mol) are reached, ca. 2 kcal/mol larger than the predicted by M06-2X and ωB97X-D. As Bickelhaupt and coworkers discussed, B3LYP often fails to reproduce the reaction barrier [77] so that this outcome is unsurprising. Additionally, these authors demonstrated that B3LYP is not adequate for mimicking biological systems involving π-stacking interactions [82]. Interestingly, B3LYP seems to overestimate the reactions barrier for the Mg-induced PT, an unexpected error sign. B3LYP is probably not adequate for the study of stacked DNA. We have also evaluated the performance of BP86 (method 5). Unlike methods 1–4, where two well-defined minima and one transition state are found, method 5 produces a rather erratic dependence of the energy along the H1 PT. This markedly different behavior arises from the changes in the hydration pattern of the central GC base pair. As shown in Fig. 4, the water molecule close to O2(C) site (see Fig. 1) "escapes" from the central base pairs and goes toward one of the borders in the Mg–GC1 form. As a consequence, the observed energy oscillation results from the combination of two effects (the tautomeric equilibrium and the change in the hydration shell), which prevents an adequate comparison of its energies. Of course, we could have frozen the position of this water molecule, but we wished to illustrate the difficulty to reach valuable results. It should also be noted that, though BP86 has been shown to adequately describe interbase bonds in gas-phase and microsolvated single base pairs [113–116], it fails in the description of stacking interactions in DNA [76, 82]. This finding clearly reflects that the performance of DFT for DNA is connected to the nature of the selected chemical model. Our ONIOM results suggest that both M06-2X and ωB97X-D functionals provide a consistent description of the induced Mg–PT process.

Eventually, we compare ONIOM results with single-point calculations at MP2/6-31G(d)(0.25). The MP2

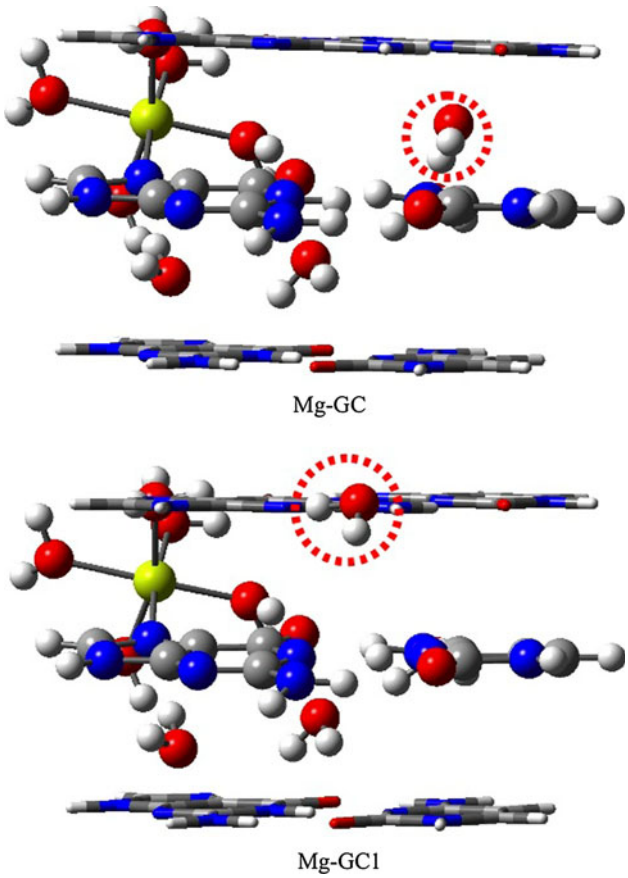

Fig. 4 ONIOM(BP86:B97-D) optimized structures for the canonical and rare tautomer forms, Mg-GC and Mg-GC1, respectively. The *circles* highlight the position of the "moving" water molecule

relative energies for the transition state and rare tautomer are 2.47 and 0.34 kcal/mol, respectively. These values are significantly below than their DFT counterparts. Precisely, the predicted energy for the transition state is ca. 6 kcal/mol smaller than the M06-2X and ωB97X-D data. Furthermore, according to this MP2 approach, the rare tautomer is practically isoenergetic with the canonical form, a rather unexpected result. Although the MP2/6-31G(d)(0.25) approach accurately describes the stacking effect [94, 95], we attribute the origin of such discrepancy to the size of the basis set. Indeed, MP2 calculations show a larger dependence with respect to basis set size than the DFT approaches when applied to stacked systems [117]. To verify this point, MP2 calculations with larger basis set would be necessary but are, unfortunately, computationally impossible due the size of the system.

3.2 The low layer method

Comparison between methods 1, 7, and 8 allow to assess the influence of the selected method in the description of the border base pairs effects. As shown in Table 1, in these

Table 3 Computed relative energies (ΔE in kcal/mol) along H1 proton transfer with selected low layer methods. The interbase bonds (in Å) are also listed

	Method				
	1	7	8	9	10
Mg–GC					
ΔE	0.00	0.00	0.00	0.00	0.00
O6(G)–N4(C)	2.84	2.82	2.80		2.87
N1(G)–N3(C)	2.95	2.94	2.92		2.93
N2(G)–O2(C)	2.98	2.98	2.96		2.90
Mg–GC1‡					
ΔE	8.04	7.74	3.69	6.90	8.02
O6(G)–N4(C)	2.65	2.65	2.63		2.67
N1(G)–N3(C)	2.69	2.69	2.68		2.68
N2(G)–O2(C)	2.91	2.91	2.92		2.86
Mg–GC1					
ΔE	3.24	3.14	3.68	1.49	2.99
O6(G)–N4(C)	2.67	2.65	2.67		2.70
N1(G)–N3(C)	2.87	2.86	2.87		2.87
N2(G)–O2(C)	3.03	3.03	3.03		2.99

methods, the same functional (M06-2X) is used in the high layer, whereas the low layer is treated with the B97-D (method 1) and M06-2X (method 7) functionals, as well as with the semiempirical PM6 model (method 8) [118]. According to the values listed in Table 3 and plotted in Fig. 5, methods 1 and 7 provide very similar results for both optimized geometries and relative energies. Indeed, the predicted interbase bonds distances are practically the same, whereas the difference in the relative energies is smaller than 0.30 kcal/mol. Therefore, M06-2X and B97-D similarly describe the stacking effects and, consequently, both methods could be used for the description of the low layer, though B97-D is apparently not adequate to model the region where PT reaction takes place as discussed above.

Moving to the PM6 description of border base pairs, we observe that the relative energy of the rare tautomer agrees with the more refined DFT calculations, while the transition state is dramatically stabilized. Consequently, the transition state and the rare tautomers structures are nearly isoenergetic. Like for method 5, this is a consequence of the changes in the hydration pattern: one of the water molecules moves from the N4(C)H_4· site to the metal hydration shell. Since the evolution of the relative energies does not reflect exclusively the H1 proton transference, the energy of the calculated Mg–GC1‡ structure cannot be used for the study of the metal-induced PT. For this reason, the complete PM6 scan was not performed.

Our calculations reveal an inherent limitation of the local microhydrated model: the optimized positions for the water molecules are deeply connected to the selected methods, which eventually affect the stability of the entire system. Such limitation could be overtaken by increasing the number of water molecules, for example, including the first hydration water molecules for the border basis pairs or by adding constraints, but at the price of more demanding calculations or less satisfying simulations. Alternatively, one can rely on a partial hydration model as the one of Fig. 2, but it is necessary to systematically check that there are no changes in the hydration pattern resulting from the PT.

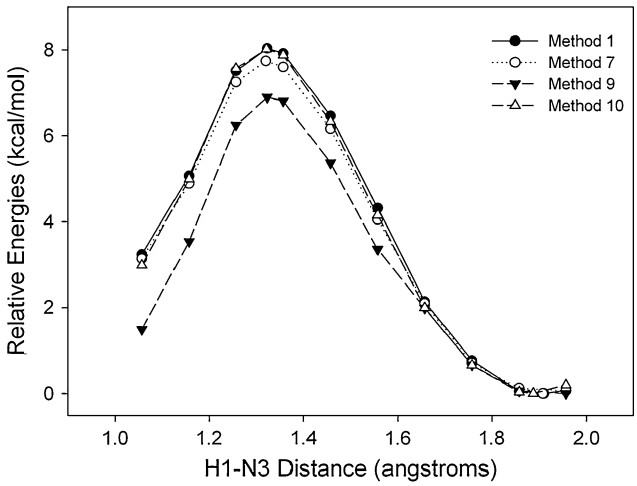

Fig. 5 ONIOM potential energy curves along the H1 proton transfer with methods 1, 7 and 9

3.3 Continuum solvent models

We have evaluated the impact of the aqueous environment beyond the first hydration by combining the explicit nine water molecules to the PCM model. First, PCM corrections are included through single-point energy calculations (method 9) performed on the geometries of method 1. As shown Fig. 5, consideration of the continuum solvent gives a small stabilization (ca. 2 kcal/mol) for both Mg–GC1‡ and Mg–GC1 with respect to the PCM-free model, which is consistent with the larger charge separation in these two cases compared to the canonical structure. However, when PCM corrections are included during the optimization (method 10), the bulk solvent effects are in fact less important. As shown in Table 3, the differences between method 1 (without PCM correction) and method 10 (PCM optimization) are less than 0.30 kcal/mol. Furthermore, practically the same hydrogen bond distances are obtained with both methods 1 and 10, and only a slight increase of the O6(G)–N4(C) and decrease of N1(G)–N3(C) and N2(G)–O2(C) bond lengths are observed. Overall, the PCM optimization provides the same picture for the

structural changes induced by PT reaction as in the original method, as evidenced by Fig. 5. This finding suggests that explicit solvent model could be enough to reproduce the main effects of solution in the induced PT, at least for the comparison of the relative energies between different tautomers of the same base pairs.

3.4 Biological implications

To clarify the actual impact of the theoretical approaches in the predicted magnesium–DNA interactions, we use methods 1–5 to calculate the PT equilibrium constant (K_{eq}) as well as the forward (k_f) and reverse (k_r) rate constants at 298.15 K. For the latter, we considered tunneling effects by introducing the Wigner term correction [119–121] in the conventional transition state theory:

$$k = \left(1 + \frac{1}{24}\left[\frac{h|\nu|}{k_B T}\right]^2\right)\frac{k_B T}{h} e^{-\Delta G^{\ddagger}/RT} \quad (1)$$

where $|\nu|$ is the (imaginary) frequency characteristic of the transition state, h is the Planck's constant, k_B is de Boltzmann's constant, and $\Delta G^{\ddagger}$ is the activation Gibbs free energy.

As showed in Table 4, the order of the predicted equilibrium constant range between 10^{-1} and 10^{-4}, depending on the method, which significantly exceeds the natural mutation rate, between 10^{-8} and 10^{-10} [122] when no bonding between DNA and metals cations is considered. Moreover, the forward rate constants, which lies in the range of 10^{7}–10^{11} s^{-1}, are large enough to allow the formation of the Mg–GC1 structure during the cell life [40]. Particularly, the extreme values agrees with our previous discussion: on the one hand, smallest k_f ($\sim 10^{7}$ s^{-1}) correspond to the method 4 (B3LYP), which overestimates the potential energy barrier, and on the other hand, method 5 (BP86) provides the largest k_f ($\sim 10^{11}$ s^{-1}) due to the change in the hydration pattern. Accordingly, all methods (including the most accurate methods 1 and 2) predict a high mutagenicity effect of the Mg^{2+}. This conclusion seems to contrast with the reality: magnesium is essential for the life and its adverse effects appears only at large doses. To explain this a priori conflicting result between theory and experience it should be noted the short life time of the Mg–GC1 form that can be quantified by means of the reverse rate constant (k_r). As Florián and Leszczyński demonstrated, only rare tautomers associated to a enough stable minimum of energy may yield permanent genetic errors [40]. According to the energetics requirements related to the time for DNA replication process, if the reverse rate constant exceeds ca. 10^{10} s^{-1}, the lifetime of the rare tautomer will be too short to induce a mutation [40]. The reverse constants listed in Table 4 rise above that limit regardless the selected high-layer method, and therefore, Mg–GC1 will reverts so quickly to the canonical structure that its impact on life is rather negligible. To confirm our results, we have also considered the tunneling correction method by Skodje and Truhlar, which depends not only on the imaginary frequency of the transition state but also on the energy barrier [123]. It is observed that both corrections predict reverse rate constants with the same order of magnitudes (e.g. 2.35×10^{11} and 2.64×10^{11} s^{-1} for method 2 and 3, respectively), with the only exception of method 1, for which the Skodje and Truhlar correction gives rise to $k_r = 1.36 \times 10^{11}$ s^{-1}. However, this finding is consistent with the good agreement between both tunneling corrections since the Wigner-corrected value is close to this order of magnitude (9.72×10^{10} s^{-1}). Finally, we notice that none of the methods are in total agreement in the magnitudes of rate and equilibrium constant, which clearly shows that the selected methods have a decisive impact on the study of metal–DNA interactions, and therefore, DFT functionals need to be cautiously combined. Among selected ONIOM schemes, methods 1 and 2 provide a similar picture of the magnesium effects, showing the reliability of the M06-2X and ωB97X-D functionals to perform these calculations.

Table 4 Calculated activation and reaction Gibbs free Energies at 298.15 K ($\Delta G^{\ddagger}$ and ΔG, respectively, in kcal/mol), forward and reverse rate constants (k_f and k_r, respectively, in s^{-1}) and equilibrium constants (K_{eq}) along the PT reaction

Method	$\Delta G^{\ddagger}$	ΔG	k_f	k_r	K_{eq}
1	5.02	1.98	3.44×10^{9}	9.72×10^{10}	3.54×10^{-2}
2	6.48	3.51	3.42×10^{8}	1.29×10^{11}	2.65×10^{-3}
3	3.25	1.16	6.51×10^{10}	4.63×10^{11}	1.41×10^{-1}
4	7.19	4.68	9.75×10^{7}	2.66×10^{11}	3.67×10^{-4}
5	2.54	2.00	2.01×10^{11}	5.93×10^{12}	3.39×10^{-2}

4 Conclusions

In this work, we have compared the description of DFT functionals for investigating PT reaction related to the metalation of nucleic acids. To this end, a chemical model that accounts for the main interactions inside DNA, namely hydration, interbase bonds and base stacking, has been used. Our calculations hints that both the B3LYP and BP86 functionals are probably not adequate to describe the PT transition state in DNA bases when applied in a ONIOM scheme. Since the barrier for the H1 PT is crucial for the stability of rare tautomeric form and hence for the possible biological impact of Mg^{2+}, alternative approaches offer a better compromise. As the M06-2X and ωB97X-D yield

consistent results and have been shown previously to adequately model biochemical systems, this work corroborates the improved performance of refined hybrid functionals in the description of PT reactions. With respect to stacking effect, the pure dispersion-corrected B97-D functional provides a description for the border base pairs similar to the one of M06-2X. However, B97-D underestimates the energetic barrier and therefore it should be used cautiously for the description of the region where PT reactions takes place. Our calculations also revealed the decisive influence of the water molecules position in the PT energetic profile of the PT transition state as well as the relative small impact of bulk solvent effects on relative energies. Indeed, very similar results are obtained with or without PCM corrections once full geometry optimizations are carried out. We conclude that the predicted biological role of the magnesium strongly depends on the selected level of theory. This investigation is an illustration that the developments of new efficient functionals allows to tackle key biological problems.

Acknowledgments J.P.C.C. acknowledges the *Région des Pays de la Loire* and the fellowship provided by the Fundación Séneca, Agencia de Ciencia y Tecnología de la Región de Murcia, within its Postdoctoral Research Staff Training Program. D.J. is indebted to the *Région des Pays de la Loire* for financial support in the framework of a *recrutement sur poste stratégique*. The work was partially supported by the Fundación Séneca del Centro de Coordinación de la Investigación de la Región de Murcia under Project 08735/PI/08, and by the Ministerio de Educación y Ciencia of Spain under Projects CTQ2007-66528 and CONSOLIDER CSD2009-00038. This research used resources of (1) the CCIPL (*Centre de Calcul Intensif des Pays de Loire*) and (2) the GENCI-CINES/IDRIS (Grant C201108547).

References

1. Santoro F, Barone V, Improta R (2007) Proc Natl Acad Sci USA 104:9931–9936
2. Improta R, Barone V (2008) Theor Chem Acc 120:491–497
3. Improta R, Santoro F, Barone V, Lami A (2009) J Phys Chem A 113:15346–15354
4. Santoro F, Barone V, Improta R (2009) J Am Chem Soc 131:15232–15245
5. Santoro F, Barone V, Lami A, Improta R (2010) Phys Chem Chem Phys 12:4934–4948
6. Improta R, Scalmani G, Barone V (2000) Int J Mass Spectrom 201:321–336
7. Xerri B, Morell C, Grand A, Gadet J, Cimino P, Barone V (2006) Org Biomol Chem 4:3986–3992
8. Labet V, Morell C, Gran A, Cadet J, Cimino P, Barone V (2008) Org Biomol Chem 6:3300–3305
9. Müller J (2010) Metallomics 2:318–327
10. Hanna R, Doudna JA (2000) Curr Opin Chem Biol 4:166–170
11. Serebrov V, Clarke RJ, Gross HJ, Kisselev L (2001) Biochemistry 40:6688–6698
12. Anastassopoulou J (2003) J Mol Struct 651(653):19–26
13. Aich P, Dasgupta D (1995) Biochemistry 34:1376–1385
14. Huang HW, Li D, Cowan JA (1995) Biochimie 77:729–738
15. Keniry MA, Owen EA, Shafer RH (2000) Biopolymers 54:104–114
16. Sreedhara A, Cowan JA (2002) Biometals 15:221–223
17. Chen SY, Lin TH (2005) J Phys Chem B 109:9764–9772
18. Barceló F, Ortiz-Lombardía M, Martorell M, Oliver M, Méndez C, Salas JA, Portugal J (2010) Biochemistry 49:10543–10552
19. Rude RK, Singer FR (1981) Annu Rev Med 32:245–259
20. Chiu TK, Dickerson RE (2000) J Mol Biol 301:915–945
21. Egli M (2002) Chem Biol 9:277–286
22. Anastassopoulou J, Theophanides T (2002) Crit Rev Oncol Hematol 42:79–91
23. Bregadze VG, Gelagutashvili ES, Tsakadze KJ, Melikishvili SZ (2008) Chem Biodiv 5:1980–1989
24. Buckin VA, Tran H, Morozov V, Marky LA (1996) J Am Chem Soc 118:7033–7039
25. Kankia BI, Marky LA (1999) J Phys Chem B 103:8759–8767
26. Serganov A, Polonskaia A, Phan AT, Breaker RR, Patel DJ (2006) Nature 441:1167–1171
27. Every AE, Russu IM (2008) J Phys Chem B 112:7689–7695
28. Ruan C, Rodgers MT (2009) J Am Chem Soc 131:10918–10928
29. Russo N, Toscano M, Grand A (2001) J Am Chem Soc 123:10272–10279
30. Russo N, Toscano M, Grand A (2001) J Phys Chem B 105:4735–4741
31. Petrov AS, Lamm G, Pack GR (2002) J Phys Chem B 106:3294–3300
32. Burda JV, Šponer J, Hrabáková J, Zeizinger M, Leszczynski J (2003) J Phys Chem B 107:5349–5356
33. Burda J, Shukla MK, Leszczynski J (2005) J Mol Model 11:362–369
34. Šponer J, Lankas F (eds) (2006) . Computational Studies of RNA and DNA. Springer, Berlin, pp 411–432
35. Michalkova A, Kosenkov D, Gorb L, Leszczynski J (2008) J Phys Chem B 112:8624–8633
36. Noguera M, Bertrán J, Sodupe M (2008) J Phys Chem B 112:4817–4825
37. Noy A, Soteras I, Luque FJ, Orozco M (2009) Phys Chem Chem Phys 11:10596–10607
38. Šponer J, Sabat M, Burda JV, Leszczynski J, Hobza P (1999) J Phys Chem B 103:2528–2534
39. Muñoz J, Šponer J, Hobza P, Orozco M, Luque FJ (2001) J Phys Chem B 105:6051–6060
40. Florián J, Leszczyński J (1996) J Am Chem Soc 118:3010–3017
41. Guallar V, Douhal A, Moreno M, Lluch JM (1999) J Phys Chem A 103:6251–6256
42. Dannenberg JJ, Tomasz M (2000) J Am Chem Soc 122:2062–2068
43. Golo VL, Volkov YS (2003) Int J Mod Phys C 14:133–156
44. Gorb L, Podolyan Y, Dziekonski P, Sokalski WA, Leszczyński J (2004) J Am Chem Soc 126:10119–10129
45. Gervasio FL, Laio A, Iannuzzi M, Parrinello M (2004) Chem Eur J 10:4846–4852
46. Perun S, Sobolewski AL, Domcke W (2006) J Phys Chem A 110:9031–9038
47. Herrera B, Toro-Labbe A (2007) J Phys Chem A 111:5921–5926
48. Villani G (2010) J Phys Chem B 114:9653–9662
49. Pérez A, Tuckerman ME, Hjalmarson HP, von Lilienfeld OA (2010) J Am Chem Soc 132:11510–11515
50. Dedíková P, Neogrády P, Urban M (2011) J Phys Chem A 115:2350–2358
51. Basch H, Krauss M, Stevens WJ (1985) J Am Chem Soc 107:7267–7271
52. Schröder G, Lippert B, Sabat M, Lock CJL, Faggiani R, Song B, Sigel H (1995) J Chem Soc Dalton Trans 23:3767–3775
53. Song B, Zhao J, Griesser R, Meiser C, Sigel H, Lippert B (1999) Chem Eur J 5:2374–2387
54. Šponer J, Šponer JE, Gorb L, Leszczynski J, Lippert B (1999) J Phys Chem A 103:11406–11413

55. Noguera M, Bertran J, Sodupe M (2004) J Phys Chem A 108:333–341
56. Matsui T, Shigeta Y, Hirao K (2006) Chem Phys Lett 423:331–334
57. Matsui T, Shigeta Y, Hirao K (2007) J Phys Chem B 111:1176–1181
58. Šponer J, Sabat M, Gorb L, Leszczynski J, Lippert B, Hobza P (2000) J Phys Chem B 104:7535–7544
59. Cerón-Carrasco JP, Zúñiga J, Requena A, Perpète EA, Michaux C, Jacquemin D (2011) Phys Chem Chem Phys 13:14585–14589
60. Gil A, Branchadell V, Bertran J, Oliva A (2009) J Phys Chem B 113:4907–4914
61. Cauët E, Liévin J (2009) J Phys Chem A 113:9881–9890
62. Cauët E, Valiev M, Weare JH (2010) J Phys Chem B 114:5886–5894
63. Acosta-Silva C, Branchadell V, Bertran J, Oliva A (2010) J Phys Chem B 114:10217–10227
64. Chen HY, Kao CL, Hsu SCN (2009) J Am Chem Soc 131:15930–15938
65. Chen HY, Yeh SW, Hsu SCN, Kao CL, Dong TY (2011) Phys Chem Chem Phys 13:2674–2681
66. Šponer J, Burda JV, Sabat M, Leszczyński J, Hobza P (1998) J Phys Chem A 102:5951–5957
67. Cerón-Carrasco JP, Requena A, Zúñiga J, Michaux C, Perpète EA, Jacquemin D (2009) J Phys Chem A 113:10549–10556
68. Solt I, Simon I, Császár AG, Fuxreiter M (2007) J Phys Chem B 111:6272–6279
69. Schneider B, Berman HM (1995) Biophys J 69:2661–2669
70. Auffinger P, Westhof E (2000) J Mol Biol 300:1113–1131
71. Makarov V, Pettitt B, Feig M (2002) Acc Chem Res 35:376–384
72. Dapprich S, Komáromi I, Byun KS, Morokuma K, Frisch MJ (1999) J Mol Struct (Theochem) 462:1–21
73. Gaussian 09, Revision B01, Frisch MJ, Trucks GW, Schlegel HB, Scuseria GE, Robb MA, Cheeseman JR, Scalmani G, Barone V, Mennucci B, Petersson GA, Nakatsuji H, Caricato M, Li X, Hratchian HP, Izmaylov AF, Bloino J, Zheng G, Sonnenberg JL, Hada M, Ehara M, Toyota K, Fukuda R, Hasegawa J, Ishida M, Nakajima T, Honda Y, Kitao O, Nakai H, Vreven T, Montgomery JA Jr, Peralta JE, Ogliaro F, Bearpark M, Heyd JJ, Brothers E, Kudin KN, Staroverov VN, Kobayashi R, Normand J, Raghavachari K, Rendell A, Burant JC, Iyengar SS, Tomasi J, Cossi M, Rega N, Millam JM, Klene M, Knox JE, Cross JB, Bakken V, Adamo C, Jaramillo J, Gomperts R, Stratmann RE, Yazyev O, Austin AJ, Cammi R, Pomelli C, Ochterski JW, Martin RL, Morokuma K, Zakrzewski VG, Voth GA, Salvador P, Dannenberg JJ, Dapprich S, Daniels AD, Farkas Ö, Foresman JB, Ortiz JV, Cioslowski J, Fox DJ, Gaussian, Inc, Wallingford CT, 2010
74. Šponer J, Riley KE, Hobza P (2008) Phys Chem Chem Phys 10:2595–2610
75. Hobza P, Šponer J (2002) J Am Chem Soc 124:11802–11808
76. Zhao Y, Truhlar DG (2005) Phys Chem Chem Phys 7:2701–2705
77. van der Wijst T, Fonseca-Guerra C, Swart M, Bickelhaupt F (2006) Chem Phys Lett 426:415–421
78. Grimme S (2004) J Comput Chem 25:1463–1473
79. Riley KE, Vondrášek J, Hobza P (2007) Phys Chem Chem Phys 9:5555–5560
80. Noguera M, Ríos-Font R, Rodríguez-Santiago L, Solans-Monfort X, Oliva A, Bertran J, Sodupe M (2009) Theor Chem Acc 123:105–111
81. Antony J, Brüske B, Grimme S (2009) Phys Chem Chem Phys 11:8440–8447
82. Fonseca-Guerra C, van der Wijst T, Poater J, Swart M, Bickelhaupt FM (2010) Theor Chem Acc 125:245–252
83. Zhao Y, Schultz NE, Truhlar DG (2006) J Chem Theory Comput 2:364–382
84. Zhao Y, Schultz NE, Truhlar DG (2008) Acc Chem Res 41:157–167
85. Zhao Y, Truhlar DG (2008) Theor Chem Acc 120:215–241
86. Becke A (1986) J Chem Phys 84:4524–4529
87. Perdew J (1986) Phys Rev B 33:8822–8824
88. Grimme S (2006) J Comput Chem 27:1787–1799
89. Lee C, Yang W, Parr R (1988) Phys Rev B 37:785–789
90. Becke A (1993) J Chem Phys 98:1372–1377
91. Zhao Y, Truhlar DG (2011) Chem Phys Lett 502:1–13
92. Chai JD, Head-Gordon M (2008) Phys Chem Chem Phys 10:6615–6620
93. Valero R, Gomes JRB, Thrular DG, Illas F (2008) J Chem Phys 129:124710
94. Hobza P, Šponer J, Polasek M (1995) J Am Chem Soc 117:792–798
95. Šponer J, Leszczyński J, Hobza P (1996) J Phys Chem 100:5590–5596
96. Jurečka P, Šponer J, Hobza P (2004) J Phys Chem B 108:5466–5471
97. Šponer J, Jurečka P, Marchan I, Luque FJ, Orozco M, Hobza P (2006) Chem Eur J 12:2854–2865
98. Alemán C (1999) Chem Phys 244:151–162
99. Alemán C (2000) Chem Phys 253:13–19
100. Oliva R, Cavallo L (2009) J Phys Chem B 113:15670–15678
101. Tomasi J, Bonaccorsi R, Cammi R, del Valle FO (1991) J Mol Struct (THEOCHEM) 234:401–424
102. Cammi R, Tomasi J (1995) J Comput Chem 16:1449–1458
103. Tomasi J, Mennucci B, Cammi R (2005) Chem Rev 105:2999–3093
104. Hohenstein EG, Chill ST, Sherrill CD (2008) J Chem Theory Comput 4:1996–2000
105. Shukla MK, Leszczyński J (2010) Mol Phys 108:3131–3146
106. Paukku Y, Hill G (2011) J Phys Chem A 115:4804–4810
107. Kumar A, Sevilla MD (2011) J Phys Chem B 115:4990–5000
108. Zhao Y, Truhlar DG (2011) J Chem Theory Comput 7:669–676
109. Dabkowska I, Jurečka P, Hobza P (2005) J Chem Phys 122:204322
110. Jurečka P, Šponer J, Hobza P (2006) Phys Chem Chem Phys 8:1985–1993
111. Barone V, Orlandini L, Adamo C (1994) Chem Phys Lett 231:295–300
112. Barone V, Orlandini L, Adamo C (1995) Int J Quantum Chem 56:697–705
113. Fonseca-Guerra C, Bickelhaupt F, Snijders J, Baerends E (2000) J Am Chem Soc 122:4117–4128
114. Fonseca-Guerra C, Bickelhaupt FM (2002) Angew Chem Int Ed 41:2092–2095
115. Cerón-Carrasco JP, Requena A, Michaux C, Perpète EA, Jacquemin D (2009) J Phys Chem A 113:7892–7898
116. Cerón-Carrasco JP, Requena A, Michaux C, Perpète EA, Jacquemin D (2009) Chem Phys Lett 484:64–68
117. Gu J, Wang J, Leszczynski J, Xie Y, Schaefer-III HF (2008) Chem Phys Lett 459:164–166
118. Řezáč J, Fanfrlík J, Salahub D, Hobza P (2009) J Chem Theory Comput 5:1749–1760
119. Wigner EZ (1941) Phys Chem 19:203–216
120. Jolibois F, Grand A, Cadet J, Adamo C, Barone V (1999) Chem Phys Lett 301:255–262
121. Di Labio GA, Johnson ER (2007) J Am Chem Soc 129:6199–6203
122. Topal MD, Fresco JR (1976) Nature 263:285–289
123. Skodje RT, Truhlar DG (1981) J Phys Chem 85:624–628